Mesoscale processes regulating the upper layer dynamics of Andaman waters during winter monsoon

*Salini.T.C[1], Smitha.B.R[2], Sajeev.R[1], Lix John. K[1], Midhunshah Hussain[1], Rafeeq.M[2]

1 Cochin University of Science and Technology, Kochi, 682016, India

2 Centre for Marine Living Resources & Ecology, Kochi, 682037, India

*Corresponding Author. email: salinitc@gmail.com, ph.+91 984688249

Abstract

The characteristics of cold core eddies and its influence on the hydrodynamics and biological production in Andaman waters were studied using insitu and satellite observations. The specific structure and patterns of the temperature-salinity (T-S) profiles, nutrients and chl a indicate the occurrence of the eddy, the spatial extent of which is well marked in sea surface height anomaly (SSHA). The Cyclonic Eddies are tracked using Okubo-Weiss parameter of $^{-}2x10^{-11}$ /s^2 centered at 8°N and 92°E, and 13°N and 93°E (CE1 and CE2 respectively). Insitu measurements are done in the eastern flank CE1 along 8°N and 92.5-93.5°E. Vertical currents recorded using Acoustic Doppler Current Profiles (ADCP) shows northward flow along the track (0.3m/s) while along the western flank, the flow is weak and southward. This evidence the occurrence of cyclonic eddy and the altimetry derived SSHA depicts the spatial extent. Analysis to explore the possible forcings to induce the occurrence of eddy, indicate baroclinic instability (Ri <0.0001) in the water column due to vertical shear in the horizontal flow. The presence of Bay of Bengal (BoB) water in the region as evidenced in the T-S profiles, and the presence of semiannual Rossby waves in the region accounts the contribution, whereas, wind stress curl was not a major inductive of divergence in the region. Though less significant, the eddy is formed to influence the nutrient pattern (NO_2, NO_3, PO_4 and SiO_4) and the biological production (chl a). The eddy influenced the nutrient pattern (NO_2, NO_3, PO_4 and SiO_4) and the biological production (chl a) in the region. CE2 is associated with convective mixing processes occurring along the northwest coast of Andaman due to the prevalent cold dry continental air from north east.

Introduction

The Sea around the Andaman and Nicobar Island chain is influenced by reversing monsoon with moisture rich summer winds and dry continental air flow from north-east during winter (Potemra et al., 1991). The region receives enormous runoff and suspended matter from Ayeyarwady-Salween river system, which has significant influence on the hydro-dynamics and oceanography (Robinson et al., 2007). The region is characterised by strong stratification, prevents vertical mixing, causes nutrient depletion in the upper layers and subsequently leads to oligotrophy. The seasonal winds, moderate or strong, though are experienced during the summer and winter months, are not found to exert any divergence or positive curl and nutrient pumping to enrich biological production is least encountered in these waters. The sea is less productive compared to the Arabian Sea and Bay of Bengal and average primary production during fall inter-monsoon is 283.19 mg $C/m^2/d$ followed by spring inter-monsoon (249 mg $C/m^2/d$), summer monsoon (238.98 mg $C/m^2/d$) and winter monsoon (195.47 mg $C/m^2/d$) [Sanjeevan et al., 2011]. Earlier observations show that the eastern and western part of the island chain is governed by distinct water properties where west shows typical BoB characteristics, northeast is highly influenced by the Ayeyarwady and Salween river system and the southeast by the productive environment of Malacca strait (Salini et al., 2010). The region is least explored for oceanic processes and surveys conducted so far for understanding the biodiversity and the basin scale environment associated with the living resources indicate the absence of any major or seasonal processes that result in nutrient pumping to alter production pattern. However, the emergence of satellite techniques, especially the Altimetry and Ocean Color imageries on mesoscale to basin scale, the understanding of the upper layer dynamics has been strengthened. Explanations have come on such major processes in the BoB, especially on number of eddies and gyres and also the impact of cyclones, which causes enormous mixing in its path (Nuncio and Prasanna Kumar, 2012). Eddies are mesoscale processes (50–200 km diameter) and ubiquitous feature of the ocean occurs in both clock-wise and anti-clock wise direction, resulting in convergence/divergence at the center.

Mesoscale eddies play a dominant role in transportation of salt, heat and nutrients within the ocean (Dong et al., 2014) and enhance local production in oligotrophic areas (Hyrenbach et al., 2006), ultimately influencing the production pattern in each trophic level (Bakun, 2006). Mechanisms behind the eddy formation has been suggested by many researchers; different driving mechanisms have been attributed to eddy formation, such as Ekman pumping and

remote forcing from the equatorial Kelvin wave reflecting off the eastern boundary as Rossby wave. According to Yu et al. (1999), westward propagating Rossby wave, excited by the remotely forced Kelvin wave, contribute substantially to the variability of the local circulation in ocean. Using the multilayer model, Potemra et al. (1991) described coastal Kelvin wave, which originates at the equator and propagates around the entire western perimeter of the region around both the Andaman Sea and the Bay of Bengal. Mesoscale eddies are observed in the coastal waters of the Andaman and Nicobar Islands (Hacker et al. 1998 and Chen et al. 2013) based on in situ hydrographic measurements. Burnaprathepart et al. (2010) described the presence of eddies in Andaman Sea and its role in enhancing the primary productivity synthesizing number of vertical profiles on chl a, major nutrients, temperature, as well as salinity. However, there are no comprehensive study undertaken for this region to explain the role of eddies (cold and warm cores) in the Andaman waters as a whole in regulating the available biological production. In this context it is attempted to enumerate these mesoscale processes based on SSHA imagery and geostrophic current pattern along with in situ evidences. The objective of this present study is to identify such processes in the basin, to explain the forcing mechanism and its response in column dynamics as well as biogeochemistry.

Data and Methodology

In situ measurements were taken onboard FORV *Sagar Sampada* during 21 November – 14 December 2011. The environmental characteristics are understood from station based measurements in the east and west of the island chain. However, the focus was to obtain a transect with 4 stations (Fig. 1) along the eddy. The meteorological parameters like air temperature, air pressure and humidity were also collected through the instruments/sensors attached to the IRAWS onboard in 15 minute interval. Profiles of temperature, salinity, dissolved oxygen and Sigma-t were obtained using SeaBird 911 Plus CTD with Niskin water samplers and deck unit for data acquisition. The datasets are processed for 1m bins. Salinity is also derived from water samples collected through Niskin samplers and using Guildline 8400A Autosal Salinometer to validate the CTD derived data.. Twelve numbers of 10 liter Niskin water samplers were used to collect water samples from standard depths (surface, 10, 20, 30, 50, 75, 100, 120, 150, 200, 300, 500, 750 and 1000 m) for measurements of dissolved

oxygen and nutrients. Temperature-Salinity profiles for water mass characteristics are based on averaged (climatological) data from Levitus et al. (1994). Mixed Layer Depth (MLD) is derived from CTD profiles as the depth at which the seawater density (Sigma-t) exceeds the surface density by 0.2 kg/m^3 (Sprintall and Tomczak, 1993). The Isothermal Layer Depth (ILD), the depth of the top of the thermocline, is defined as the depth at which surface temperature decreases by 1 °C from sea surface temperature (Kara et al., 2000 and Rao and Sivakumar, 2003). The thickness of the barrier layer is computed as the difference between ILD and MLD (Lukas and Lindstrom, 1991).

Monthly composite of the chlorophyll data is obtained from the Distributed Active Archive Center (DAAC) of National Aeronautics and Space Administration, NASA. Dissolved oxygen was measured by Winkler titration. Analyses of nitrite, nitrate, phosphate and silicate were performed using a Skalar Analyser.

Wind stress curl (daily) data used was taken from ASCAT processed by NOAA/NESDIS utilizing measurements from the Scatterometer instrument aboard the EUMETSAT Metop satellites with a spatial resolution of 25 km; chl a data was taken from MODIS Aqua Level 3 at a spatial resolution of 4 km, downloaded from Ocean Color Website and processed using SeaDas. SST was obtained from MODIS Aqua Level 3 at a spatial resolution of 4 km downloaded from Ocean Color Website, while SSHA data obtained with 7 day temporal resolution from AVISO for the period from January 2003-January 2013. The cold core eddy was recognized through SSHA with geostrophic current imagery obtained from https://oceanwatch.pifsc.noaa.gov, and was observed to be centered at 7° N and 90° E with current moving in cyclonic direction. Net heat flux, solar radiation, latent heat flux, and specific humidity were obtained from http://oaflux.whoi.edu.

The eddies are spotted using two ways, first method is using SSHA contours and geostrophic currents, calculated from the following geostrophic equations,

$$u = -\frac{g}{f}\frac{\partial h}{\partial y} \qquad (1)$$

$$v = \frac{g}{f}\frac{\partial h}{\partial x} \qquad (2)$$

Where u and v are the zonal and meridional components of geostrophic currents, g is the gravitational acceleration, f is the Coriolis parameter, x and y are longitudinal, latitudinal co-ordinates and h is the SSHA.

Second method is using the Okubo-Weiss parameter, OW (Okubo, 1970 and Weiss, 1991) and is defined as

$$OW = s_n^2 + s_s^2 - w^2 \qquad (3)$$

Where s_n is the normal strain component, s_s is the shear strain component and w is the relative vorticity.

$$s_n = \frac{\partial u}{\partial x} - \frac{\partial v}{\partial y} \qquad (4)$$

$$s_s = \frac{\partial v}{\partial x} + \frac{\partial u}{\partial y} \qquad (5)$$

$$w = \frac{\partial v}{\partial x} - \frac{\partial u}{\partial y} \qquad (6)$$

If the vortex core is dominated by vorticity, the negative Okubo-Weiss are predictable in the vortex core.

Wavelet transform is an appropriate analysis tool to study multi-scale, non-stationary processes occurring over finite spatial and temporal domain. In this study, the wavelet was used to analyse time series data of oceanographic parameters that contain non-stationary power at many different frequencies. This technique is used to decompose time series into its frequency components based on the convolution of the original time series with a set of wavelet functions, and if possible, determine both the dominant modes of variability, and how those modes vary with time. It expands functions in terms of wavelets, which are generated in the form of translations and dilations of a fixed function called the Mother Wavelet. In the present study the wavelet is applied to explain the temporal variation of SSHA in the eddy region to explore the life span and frequency of the processes during the 10 years.Meyers et al. (1993) used wavelet analysis to study the propagation of mixed Rossby-gravity waves in an idealized numerical model of the Indian Ocean.

The phase speed for long baroclinic Rossby wave is given by $C = \frac{-gH_0\beta}{f^2}$, (7)

where g is the reduced gravity term (taken as 0.04 m s^{-2} for the first baroclinic mode), H_0 is the thermocline depth (taken as an annual mean depth of 20°C isotherm derived from Levitus and Boyer, 1994), f the Coriolis parameter and $\beta = \frac{\partial f}{\partial \phi}$, where ϕ is the latitude.

Results and Discussion

Physical characteristics of the Eddy region

The region is characterized by warm (27.6–28 °C), humid (72–77%) air and wind is from northeast, suggesting the prevalence of northeast monsoon condition of magnitude in the range of 10–12 m/s with comparatively lower speed (10 m/s) in the western part and higher speed (12 m/s) in the eastern part of the eddy (referred to hereafter as CE1).

The SST varies in the range of 28.4-28.8 °C with lower temperatures near the coastal water compared to offshore; the surface salinity (33.00 psu) and density (20.40 kg/m^3) values, on the other hand, are similar in coastal and offshore waters. Regional water mass characteristics from temperature, salinity, and density profiles show that the area is occupied by BoB waters with temperature ranging from 28.0-28.5 °C, salinity 33.2-33.8 psu, and density 20.6-20.8 kg/m^3 (Salini et al., 2018). Vertical temperature distribution along 8°N (Fig. 2b) shows warm (>28.5 °C) and thick isothermal layer (~54 m) in the western part and a gradual decrease towards east (20 m). The most important feature in the thermal structure is the upsloping of isothermal layer, which is prominent in the subsurface (54–220 m) also, and the mixed layer depth (MLD) shoaled from west to east (47–19 m). Vertical salinity and density distribution show the presence of low saline (32.9–33.1psu) water in the upper 30 m, with an upsloping tendency (Fig. 2 c, d) as in the case of temperature. Similar pattern is reflected in density characteristics too.

The horizontal current structure at 8° N along 92.5° E to 93.5° E shows irregular current pattern from surface to 90 m (Fig. 3). Along the eastern part of the 100 km transect, major flow is towards south (≅30 km), west to it with a narrow and weak northward flow, followed by major southward drift up to 40 m. However, the response to this irregular pattern is insignificant in the T-S profiles and so the eastern part of the transect (~60 km) is not considered for addressing the eddy. In the western flank, the northward and the subsequent flow

towards south indicate cyclonic flow direction. The current recorded at 16 m depth is considered for near surface pattern and this shows the presence of a northern component with a magnitude of 0.3 m/s in the eastern part negligible speed in the western part, directed westward. But at 40 m the current magnitude decreases in the eastern flank (0.1 m/s) and increases in magnitude in the western flank (0.1 m/s) with direction changing from northeast to southwest. The current at 88 m also follows the same pattern, but magnitude changes from 0.5 m/s in the western part and 0.4 m/s in the eastern part. The upsloping in the T-S profiles concurrent to this confirms the feature as a subsurface cyclonic eddy. The flow in the eastern flank is towards north (0.3 m/s) and at west it is to the south (0.5 m/s). The data was analyzed for all 8 m cells up to 88 m depth and found to follow the same pattern as that of near surface but with a decreasing magnitude. The dataset was seen to contain spurious values below 88 m and hence discarded.

Eddy Generation Mechanism

The possible physical mechanisms that govern the eddy includes the wind stress curl, topographic instability, shear flows, baroclinic instability and the radiation of Rossby waves from poleward propagating coastal Kelvin waves etc. (White, 1977 and Kessler, 1990). Daily wind stress curl is examined to identify the local forcing that contributes to the formation and sustenance of the eddy. Curl of the eddy region from ASCAT wind data shows negative values in the range of $^{-}5.6\text{x}10^{-8}$ and $^{-}8.24\text{x}10^{-8}$ Pa/m, indicating convergence and hence the contribution due to wind stress curl is ruled out.

Other possible eddy generation mechanisms are differential mixing of region with the adjacent sea mainly through inflow from Malacca Strait and freshwater influx from adjoining rivers leading to strong density variations in the water column. This variation may reduce or enhance the mechanical effects in the form of eddy or meanders in the region. This is measured based on the estimated Richardson Number (Ri). According to Miles (1961), the flow is stable if Ri>0.25.

Ri is calculated as $\text{Ri} = \frac{\text{N}^2}{(\frac{\partial u}{\partial z})^2}$ (7)

where N^2 is the Brunt Vaisala frequency (BV),

$$N^2 = \frac{-g}{\rho_0}\frac{\partial \sigma_t}{\partial z} \quad (8)$$

where g is the gravitational acceleration, $^{\rho}{}_0$ the average sea water density, z the depth, and σ_t is ρ-1000 where ρ is the sea water density. The denominator term $\partial u/\partial z$ in (7) is the velocity gradient, which is an indicator of strength of mechanical generation calculated from vertical current profiles acquired using ADCP.

The low BV (avg. 3.165 x 10^{-5} s^{-1}) and large velocity gradient (avg. 3.968 s^{-2}) resulted into low Ri (avg. 0.0001), indicating unstable well mixed water column. These lead to instability in the water column and favor eddy-like perturbation in the region.

Instability arises either as a result of mixing of different water masses or due to the shear flows. Mixing with other water masses can be ruled out as there is clear evidence of the presence of BoB water in the eddy region from the T-S profiles. Another possibility is the prevalence of planetary waves that might modulate the horizontal flow and induce shear, thereby causing instability; such instability has been well reported along this region by Schott et al., 2009 and Rao et al., 2010, that planetary waves influence the near surface circulation through local and remote forcing. The role of such planetary wave influence on eddy generation mechanism was examined using altimeter data and mapping of planetary wave propagation was carried out to identify their influence on regional circulation. Referring to Yu (2003), Hovmuller diagram of SSHA at 8°N along 89°E to 94°E was analyzed to track the planetary wave and are plotted (Fig. 4). Low SSHA in this region from mid-November to mid-January indicates the presence of upwelling mode Rossby wave (Girishkumar et al., 2011). Negative SSHA is almost horizontal, indicating a fast propagation of Rossby wave. Further west (nearer to the eddy location), negative SSHA showed a steeper slope, indicating a slower propagation. The westward propagating signal takes about 45-60 days to travel from the coast of Nicobar Island chain (Potemra et al., 1991) to the core of the eddy region, which yields phase velocity of the westward signal at 0.20 m/s. The theoretical phase speed of Rossby wave at 8°N that propagates westwards is calculated as 0.21 m/s, suggesting that the signal appearing in the plot is a Rossby wave that is generated on the west coast of Nicobar island chain. The estimated speed of the wave is close to the theoretical wave speed and the estimate also compares well with earlier results of Yang et al. (1998), Yu (2003) and Girishkumar et al. (2011). The Rossby waves were

produced by radiation from the west coast of Nicobar Island chain in association with poleward propagating coastal Kelvin waves (Potemra et al., 1991). The baroclinic instability due to the interaction of westward propagating Rossby waves and local wind stress curl cause meanders and eddies in BoB (Nuncio and Prasanna Kumar, 2012). Using a numerical model, Kurien et al. (2010) also concluded that baroclinic instability plays a key role in meander growth and eddy generation in BoB. Sreenivas et al. (2012) argued that coastal Kelvin waves and the associated radiated Rossby waves from the east play a dominant role in the mesoscale eddy generation in BoB. Chen et al. (2012) studied the interannual variability mechanism of the mesoscale eddies in BoB and pointed that the eddy activities do not directly link to El Nino Southern Oscillation (ENSO) events and are sensitive to the baroclinic instability of the background flow.

To ascertain the periodicity of SSHA, the data is again subjected to continuous wavelet transforms with Morlet wave as mother wavelet following Torrence and Compo (1998). It is clear from Fig. 5 that the dominant mode of variability is semiannual. In the Andaman waters, the wave period is more variable due to the effect of westward propagating Rossby wave from the coastally trapped Kelvin wave (Vialard et al., 2009 and Nienhaus et al., 2012). From power and global wavelet spectrum, the predominant frequencies are in semiannual and annual modes. The annual mode seems to be reduced in intensity compared to the semiannual mode. On the basis of the results of wavelet analyses, it is clear that the semiannual Rossby waves are significant in the years 2005, 2008, 2010 and 2011, whereas the annual wavelets are significant during 2006-2009. Therefore, we concluded that the westward propagating Rossby wave radiated from the coastal Kelvin wave contribute to cyclonic eddy in the region.

Chemical and biological response of the eddy

Concurrent with the thermohaline oscillations, the vertical structure of dissolved oxygen (DO) also demonstrates fluctuations above 90 m depth. The 4.22 ml/L DO contour shoaled from a depth of about 47 m (92.3°E) to 25-30 m at eastern flank of the eddy (93.3°E). The upper nitrate (NO_3) concentration is in detectable levels (0.67-0.98 μM) and shows slight upsloping towards the eastern flank (93.3°E). The phosphate (PO_4) concentration in the upper water was also at a detectable level and showed a slight upsloping towards the eastern side (0.12 μM at 92.3°E and 0.27 μM at 93.3°E). Further, the vertical distribution of silicate (SiO_4) showed slight upsloping towards the eastern periphery (0.77 μM at 92.3°E to 1.62 μM at 93.3°E). Hence,

concomitant with the thermohaline characteristics, the vertical distribution of nutrients also showed oscillations in the upper water column.

The physical and chemical characteristics do reflect on the regional biology and this is well reflected in the surface chl a distribution. Chl a derived from ocean colour imagery (Fig. 6) can illustrate the standing stock of the primary consumers for the optical depth and is 0.5 mg/m^3 in the eddy region compared to the adjacent regions (0.1 mg/m^3). This increases within the eddy in association with the nutrient values explains the impact of churning due to the eddy. And this points out the significance of such mesoscale processes that influence the production marginally in the Andaman waters.

Satellite evidence (SSHA based) for cyclonic eddies

The distribution of mesoscale production favourable pockets is examined using monthly SSHA and geostrophic current pattern (Fig. 7a-d) for the winter monsoon (November-February, 2011). This evidences the presence of one cyclonic eddy (CE), of which CE1 is the same that encountered during the in situ measurements. CE1 was stronger as indicated by negative SSHA between 5°–9°N with core at 7° N latitude and is observed to be propagating from 93°E to 86°E within one month (November to December). The eddy intensity is more during November and December, with a negative value of -0.14m. In December CE1 propagates westward to BoB and is observed between 86°-93°E. It is completely replaced from Andaman waters by January and exhibited a positive SSHA (0.18 m). But the low SSHA observed in BoB waters even during February centered at 86° E. The shape of the eddy is elliptical with its axis oriented in east west direction. The eddy CE1 characteristics and generating mechanism is described in the above sections (3.3.1-3.3.3) using in situ as well as satellite observations.

The SSHA maps also revealed a low SSHA pocket located at 13°N and 93°E during November with negative anomaly of -0.12m. This is marked as CE2. The negative anomaly is more in November with SSHA of -0.12 m, and the intensity decreases during December with SSHA of -0.10. Negative anomaly is replaced by positive anomaly of 0.16m during January.

In order to identify eddies in a prominent way, Okubo-Weiss (OW) parameter method is also exercised in this study. Eddies are characterized with negative OW parameter at the eddy core due to the dominance of vorticity over strain components; while strain dominated areas

have positive OW parameter. According to Isern-Fontanet et al. (2003), closed contours of OW with a value of $^{-}2x10^{-11}$ $/s^2$ corresponding to the threshold value for defining eddies. The threshold value was fixed as same as Isern-Fontanet et al. (2003) for defining eddies and finding out the vorticity dominated area. From the Fig. 3.7, the closed contours of OW, and cyclonic current structure confirmed the presence of an intensified cyclonic eddy at 8°N and 93°E. But the area characterized with threshold value less than $^{-}2x10^{-11}$ $/s^2$, negative SSHA and the cyclonic current structure at 13°N and 93°E indicated the presence of a weak eddy.

Having recognized eddies from SSHA, OW and geostrophic current maps, it is further confirmed the occurrence of prevailing processes using SST and chlorophyll. Cyclonic eddies formed due to the divergent forcing at the center is occupied with sub-surface nutrient rich waters at the core. These areas of negative SSHA are characterised with relatively cool and high chlorophyll concentration.

SST is high during the initial phase of winter months, i.e. in November (Fig. 8a), with higher values in the entire region of Andaman waters (28.2-28.8 °C). During December (Fig. 8b), the values change to 27.6-28.8 °C. Further, during January (Fig. 8c) and February (Fig. 8d), the basin wide temperature is in the range to 27-29 °C and 26-29 °C respectively. Though the Andaman waters are warm in general, the cold core eddies identified in this area show relatively cool temperatures owing to the prevalent cyclonic flow associated with it. CE1 records a temperature of 28.6 °C during November, and when the eddy advances to the Andaman waters the surface temperatures begin to cool. SST decreases from 28.6 to 28.2 °C during December; SST again decreases to 27.6 °C in January. But in February the temperature remains the same as in January. CE2 displays a temperature of 28.6 °C during November; during December, the temperature decreases to 28.2 °C, and decreases further to 27 °C during January and again in February (26.5 °C). The hike in temperature along the eastern Andaman waters might be due to the intrusion of low saline waters through Malacca strait as inferred by Rama Raju et al., 1981, and Tan et al., 2006.

High chlorophyll concentration is expected in the eddy region due to enhancement of nutrients at the surface. These cold core eddies are important because they are in the area of high biological activity and these areas are observed to have strong physical and

biogeochemical coupling resulting in high chlorophyll concentration. Generally, Andaman waters are oligotrophic in nature with less chlorophyll concentrations (Vijayalakshmi et al., 2010). The existence of cyclonic circulation increases the chl a levels in the eddy region. When the cyclonic flow advances, increased chl a level was observed in the eddy locations at CE1 and CE2. CE1 recorded 0.1 mg/m^3 during November, increased to 0.8 mg/m^3 during December and decreased again to 0.3 mg/m^3 in January (Fig. 8 a-d). Chl a level decreased to 0.2 mg/m^3 in February. CE2 revealed a very low value (0.1 mg/m^3) during November; during December, chl a began to increase in the eddy region (0.4 mg/m^3) and in January also the pattern followed with a concentration of 0.4 mg/m^3, which decreased to 0.2 mg/m^3 in February.

The role of wind stress curl on inducing the eddy was verified with weekly progress in the wind stress curl (ASCAT) for the pockets. At CE1 the curl varied from $^{-}4.43x10^{-7}$ to $1.28x10^{-6}$ Pa/m, but the mode of the signal was $^{-}1.47x10^{-7}$ Pa/m. The wind curl at CE2 showed values between $^{-}2.87x10^{-7}$ and $2.09x10^{-6}$ Pa/m and mode was $^{-}3.25x10^{-8}$ Pa/m. However, the occurrence of maximum negative values implies that wind is not a dominant causative factor for the generation of eddy.

At CE2, the surface temperature is low (27-27.2 °C) compared to the nearby locations and the MLD is also deeper (>70m). Wind is northeasterly, with a magnitude of 4 to 7 m/s. Specific humidity of 14 to 18 g/kg implies dry continental air during the period. Net heat flux varies from $^{-}98$ to $^{-}134$ W/m^2 during November-February. This causes heat loss due to evaporation (latent heat flux $^{-}220$ to $^{-}312$ W/m^2), resulting in cooling in the sea surface. Solar radiation varies from 114 to 170 W/m^2 in the eddy region. This low solar insolation reduces the SST, resulting densification of water. Thus, the surface water sinks and nutrient rich water entrains from deeper depths. This evidences that the atmospheric forcing causes surface cooling and the resulting convective mixing entrains nutrients into the upper layer which activates the primary production (Prasanna Kumar and Prasad, 1996, Madhupratap et al., 1996). Chatterjee et al. (2016) reported that the equatorial signal of Kelvin comes into the Andaman Sea through the Great Channel, travels along the eastern boundary, and exits to BoB through Preparis Channel, with a smaller part flowing southward along the east coast of the Andaman Islands. In this context it is presumed that the generating mechanism of CE2 is Kelvin. The instability owing to

the flow from Ayeyarwady-Salween river system is also supposed to be the reason for CE2 origin.

Conclusion

The column dynamics, forcing mechanisms, chemical and biological responses of cyclonic eddies are explained for the Andaman waters based on a suit of in situ and satellite datasets. The eddies are tracked using Okubo-Weiss parameter and the eddy CE1 is strong compared to CE2 based on the threshold Okubo-Weiss parameter of $^{-}2x10^{-11}$ /s^2. The processes are small scale in nature within 100-350 km diameter, and are found to be induced as a result of baroclinic instability arising owing to the westward propagating Rossby wave, semi-annual mode with phase speed of 0.20 m/s for CE1 and CE2 may be induced by Kelvin and the instability occurs due to the Ayeyarwady-Salween flow. While CE2 is associated with the process of convective mixing process occurring in the region due to cold dry continental air from north east. The study concludes that, in addition to the mesoscale processes, the convective mixing occurring along the northwest coast of Andaman is taking a substantial role in triggering the biological production of Andaman waters. Considerable increases in the regional surface biological production indicates the complementary role of such processes in bringing up the quality of production in Andaman waters. The role of convective mixing and eddies in the dynamics of the Andaman waters are explained for the first time.

Acknowledgements

Authors are grateful to the Ministry of Earth Sciences for supporting the work and for providing facilities onboard FORV Sagar Sampada for in-situ measurements. All the fellow participants of the cruise FORV SS292 are thankfully acknowledged. Insitu data are obtained from FORV Data Centre in CMLRE.ASCAT Scatterometer wind field is obtained from NOAA/NESDIS. The TOPEX/Poseidon SSHA product is generated from the Merged Geophysical Data Record. Chlorophyll data was retrieved from GSFC NASA. Heat flux data is provided by WHOI OAFlux project.

References

366 Bakun, A. (2006). Fronts and Eddies as Key Structures in the Habitat of Marine Fish
367 Larvae:Opportunity, Adaptive Response and Competitive Advantage.*Scientia Marina*, 70 (S2),
368 105–122.

369 Buranapratheprat, A., Laongmanee, P., Sukramongkol, N., Prommas, R., Promjinda, S., &
370 Yanagi, T. (2010). Upwelling Induced by Mesoscale Cyclonic Eddies in the Andaman
371 Sea.*Coastal Marine Science*, 34 (1), 68–73.

372 Chen Gengxin, Wang Dongxiao & Hou Yijun. (2012). The features and interannual variability
373 mechanism of mesoscale eddies in the Bay of Bengal. *Continental Shelf Research*, 47, 178-185.

374 Chen, X., Pan, D., Bai, He, X., Chen, C.A., & Hao, Z. (2013). Episodic Phytoplankton
375 BloomEvents in the Bay of Bengal Triggered by Multiple Forcings.*Deep Sea Research Part I:*
376 *Oceanographic Research Papers*,73,17–30.

377 Dong, C., McWilliams, J.C., Liu, Y., & Chen, D (2014). Global heat and salt transports by eddy
378 movement.*Nat. Commun.*, 5, 3294.

379 Girishkumar, M.S., Ravichandran, M., McPhaden, M.J., & Rao, R.R. (2011). Intraseasonal
380 variability in barrier layerthickness in the south central Bay of Bengal. *Journal of Geophysical*
381 *Research*, 116, C03009.

382 Hacker, P., E. Firing, J. Hummon, Gordon, A.L., & Kindle, J.C. (1998). Bay of Bengal Currents
383 during the Northeast Monsoon. *Geophysical Research Letters*. 25 (15), 2769–2772.

384 Hyrenbach, K. D., Veit, R.R., Weimerskirch, H., & Hunt, G.L. (2006). Seabird Associations with
385 Mesoscale Eddies: The Subtropical Indian Ocean. *Marine Ecology Progress Series*, 324, 271–
386 279.

387 Jury, R. M., & Huang, B. (2004). The Rossby wave as a key mechanism of Indian Ocean climate
388 variability, *Deep Sea Res. Part I*, 51, 2123–2136.

389 Kessler, W. S. (1990). Observations of long Rossby waves in the northern tropical Pacific.*J.*
390 *Geophys. Res.*, 95, 5183–5217.

391 Kurien, P., Ikeda, M., & Valsala, V.K. (2010). Mesoscale variability along the east coast of India
392 in spring as revealed from satellite data and OGCM simulations, *J. Oceanogr.*, 66, 273–289.

Levitus, S., & Boyer, T. (1994). World Ocean Atlas 1994, Vol 4: Temperature, NOAA Atlas NESDIS 4, U.S. Govt. Printing Office, 150.

Levitus, S., Burgett, R., & Boyer, T. (1994): World Ocean Atlas 1994, Vol 3: Salinity, NOAA Atlas NESDIS 3, U.S. Govt. Printing Office, 150.

Madhupratap, M., Prasanna Kumar,S., Bhattathiri, P.M.A., Dileep kumar, M., Raghukumar, S., Nair., K.K.C., & Ramaiah, N. (1996). Mechanism of the biological response to winter cooling in the northeastern Arabian Sea. *Nature* ,384, 549 – 552.

Meyers, S. D., Kelly, B.G., & O'Brien, J.J. (1993). An introduction to wavelet analysis in oceanography and meteorology: With application to the dispersion of Yanai waves. *Mon. Wea. Rev.*, 121, 2858–2866.

Miles, J.W. (1961). On the stability of heterogeneous shear flows. *Journal of Fluid Mechanics*, 10, 496-508.

Nienhaus, M. J., Subrahmanyam, B., & Murty, V.S.N. (2012). Altimetric observations and model simulations of coastal Kelvin Waves in the Bay of Bengal, *Mar. Geod.*, 35(1), 190–216.

Nuncio, M., & Prasanna Kumar, S. (2012). Life cycle of eddies along the western boundary of the Bay of Bengal and their implications, *J. Marine Syst.*, 94, 9-17.

Potemra, J.T., Luther, M.E., & O'Brien, J.J. (1991). The seasonal circulation of the upper ocean in The Bay of Bengal. *Journal of Geophysical Research*, 96, 667-683.

Prasanna Kumar, S. & Prasad, T.G. (1996). Winter cooling in the northern Arabian Sea. *Current Science*, 71, 834-841.

Rama Raju, D. V., Gouveia, A. D., & Murthy, C. S. (1981). Some physical characteristics of Andaman Sea Waters during winter. *Indian Journal of Marine Sciences*, 10, 211–218.

Robinson, R.A.J., Bird, M.I., Oo, N.W, Hoey, T.B., Aye, M.M.D., Higgitt, L., Lud, X.X., Swe, A., Tun, T., & Win, S.L. (2007). The Irrawaddy river sediment flux to the Indian Ocean:the original nineteenth-century data revisited. *Journal of Geology*. 115, 629–640.

Salini, T.C., Fanimol, C.L., Smitha, B.R., Jayalakshmi, K.J., Asha Devi, C.R., Sanjeevan, V.N., Saravanane, N., & Sajeev, R. (2010). Oceanography of the Andaman Waters: Physico-chemical and biological characteristics during Januaryuary 2009. In: Indian Ocean Marine Living Resources, Book of Abstracts (Ed. G.V.M.Gupta et al), Centre for Marine Living Resources and Ecology, Ministry of Earth Sciences, Kochi, 29.

Sanjeevan, V.N., Smitha, B.R., Ashadevi, C.R., Abdul Jaleel, K.U. and Jayalalshmi, K.J., 2011. Revalidation of Potential Yield from Indian EEZ.A trophodynamic approach. *In Report of the Working Group for revalidating the potential of fishery resources in the Indian EEZ*, New Delhi.

Schott, F. A., Xie, S.P., & McCreary Jr., J.P. (2009). Indian Ocean circulation and climate variability, *Rev. Geophys.*, 47, RG1002.

Sindhu, B., Suresh, I., Unnikrishnan, A.S., Bhatkar N.V., Neetu, S., Michael, G S. (2007). Improved bathymetric datasets for the shallow water regions in the Indian Ocean. *J. Earth Syst. Sci.*, 116(3), 261-274.

Sreenivas, P., Chowdary, J.S., Gnanaseelan., C. (2012b). Impact of tropical cyclones on the intensity and phase propagation of fall Wyrtki jets.*Geophys Res. Lett.*,9,L22603.

Tan, C.K., Ishizaka, J., Matsumura, S., Md.Yusoff, F., Hj.Mohamed, & M.I. (2006). Seasonal variability of SeaWiFS chlorophyll a in the Malacca Straits in relation to Asian monsoon. *Continental Shelf Research*, 26, 168-178.

Torrence C., & Compo, G.P. (1998). A Practical Guide to Wavelet Analysis, *Bull. of the American Met. Soc.*, 79, 61-78.

Vialard, J., Shenoi, S.S.C., McCreary Jr, J.P., Shankar, D., Durand, F., Fernando, V., & Shetye, S.R. (2009). Intraseasonal response of the northern Indian Ocean coastal waveguide to the Madden-Julian Oscillation, *Geo. Phys. Res. Letts.*, 36.

Vijayalakshmi R. Nair, & Gireesh, R. (2010). Biodiversity of chaetognaths of the Andaman Sea. Indian Ocean. *Deep Sea Research II*, 57, 2135-2147.

White, W. B. (1977). Annual forcing of baroclinic long waves in the tropical North Pacific.*J. Phys. Oceanogr.*, 7, 50–61.

445 Yang, J., Yu, L., Koblinsky, C.J., & Adamec, D. (1998). Dynamics of the seasonal variations in
446 the Indian Ocean from TOPEX/POSEIDON sea surface height and an ocean model, *Geophys.*
447 *Res. Letts.*, 25 (11), 1915 - 1918.

448 Yu, L. (2003). Variability of the depth of the 20°C isotherm along 6°N in the BoB: its response
449 to remote and localforcing and its relation to satellite SSH variability. *Deep-Sea ResearchII*, 50,
450 2285–2304.

451 Yu, L. S., & Rienecker, M.M. (1999). Mechanisms for the Indian Oceanwarming during the
452 1997-98 El Nino. *Geophys. Res. Lett.*, 26 735738.

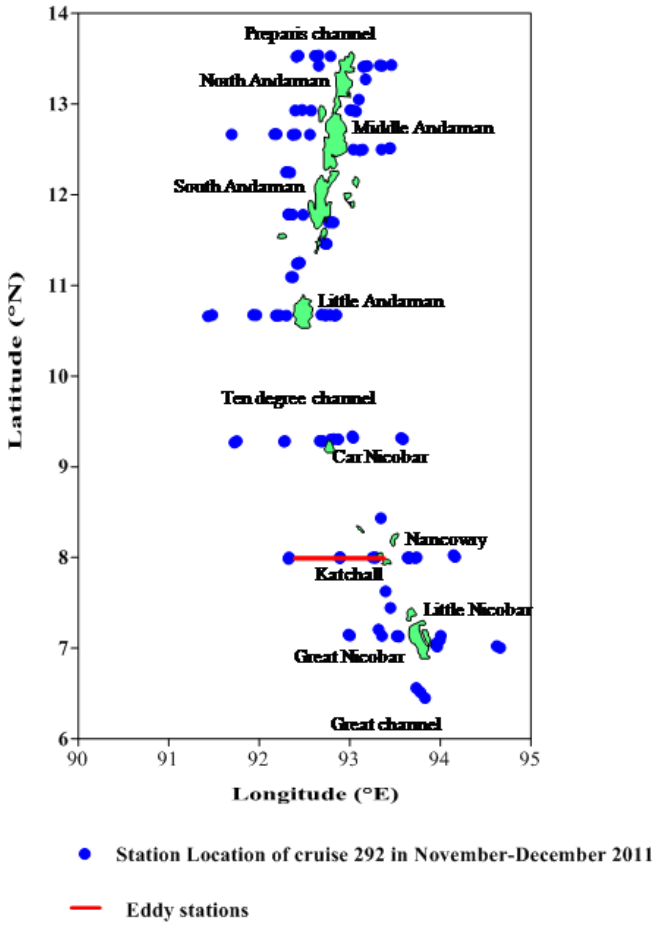

Fig. 1 Station Location

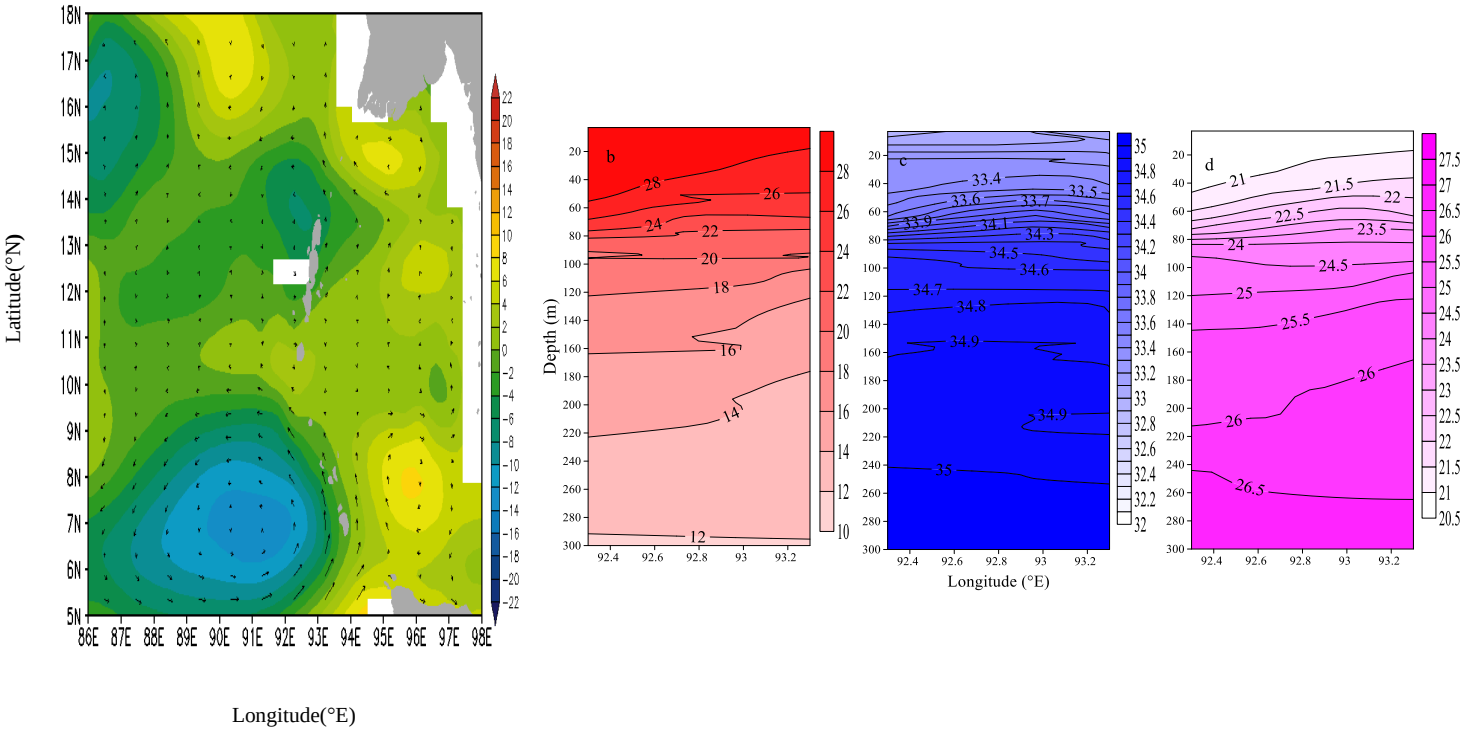

Fig. 2 a) Sea Surface Height (cm- Aviso weekly) and geostrophic current (cm/s) and the eddy location

b) Vertical temperature (°C), c) salinity and d) density (kg/m^3) distribution at the eddy location

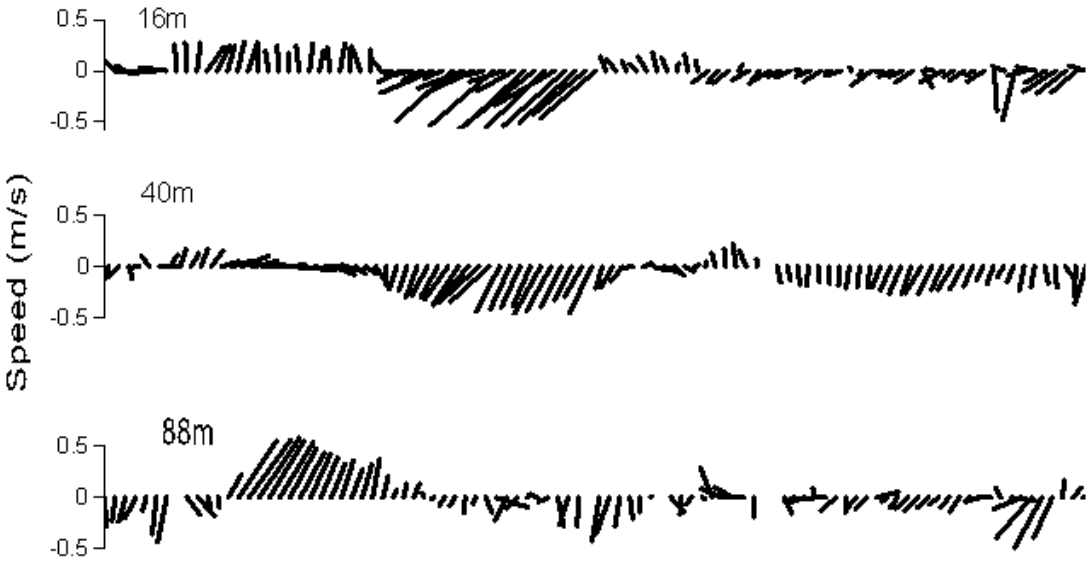

Fig. 3 Horizontal current (m/s) structure at different depths along 8°N

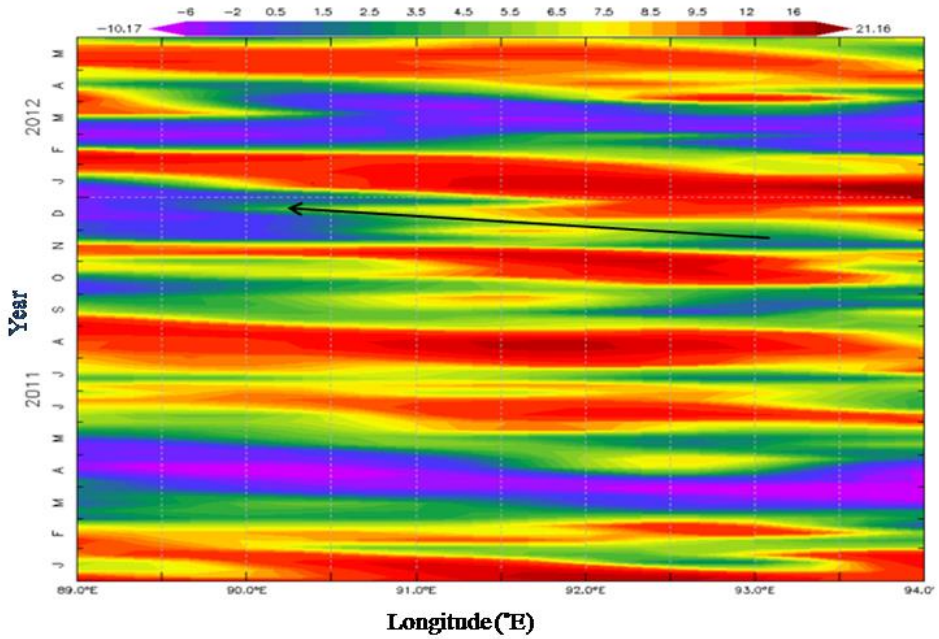

Fig. 4 Hovmuller diagram of SSHA(m) (Aviso monthly) along 8°N

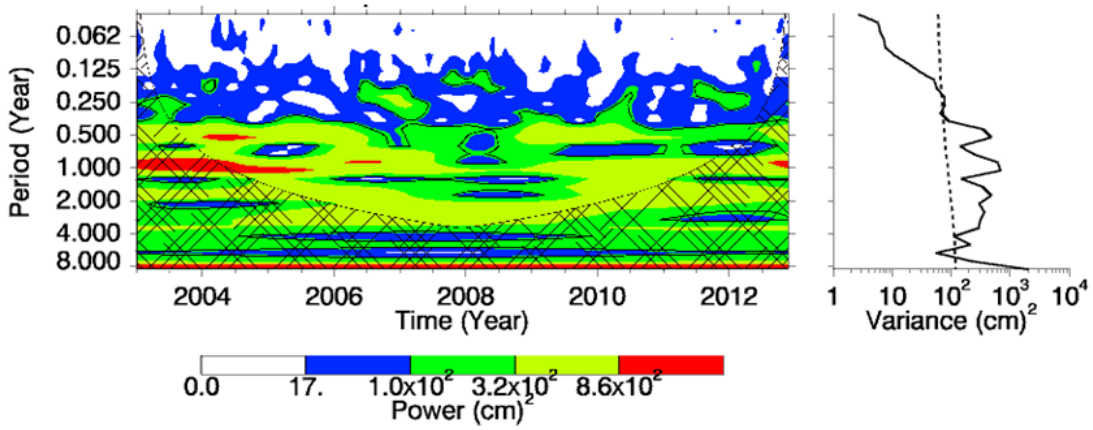

Fig. 5. Wavelet spectra of SSHA (m- Aviso monthly from 2003-2013) along 8°N

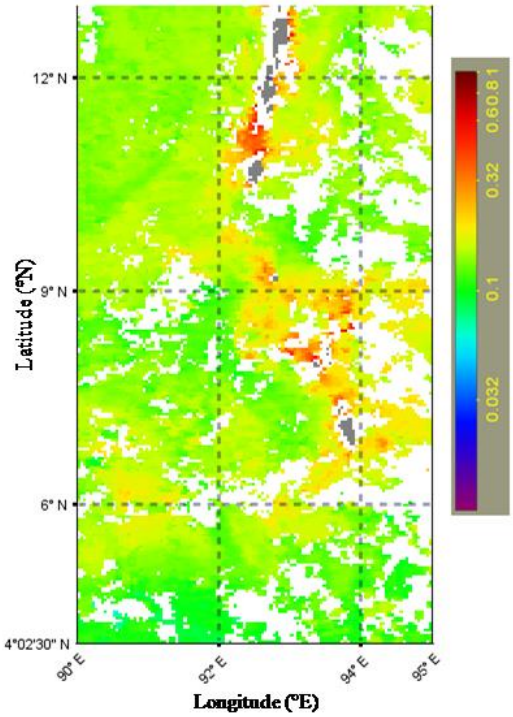

Fig. 6 chl a (mg/m^3- weekly MODIS Aqua) pattern during the insitu observation

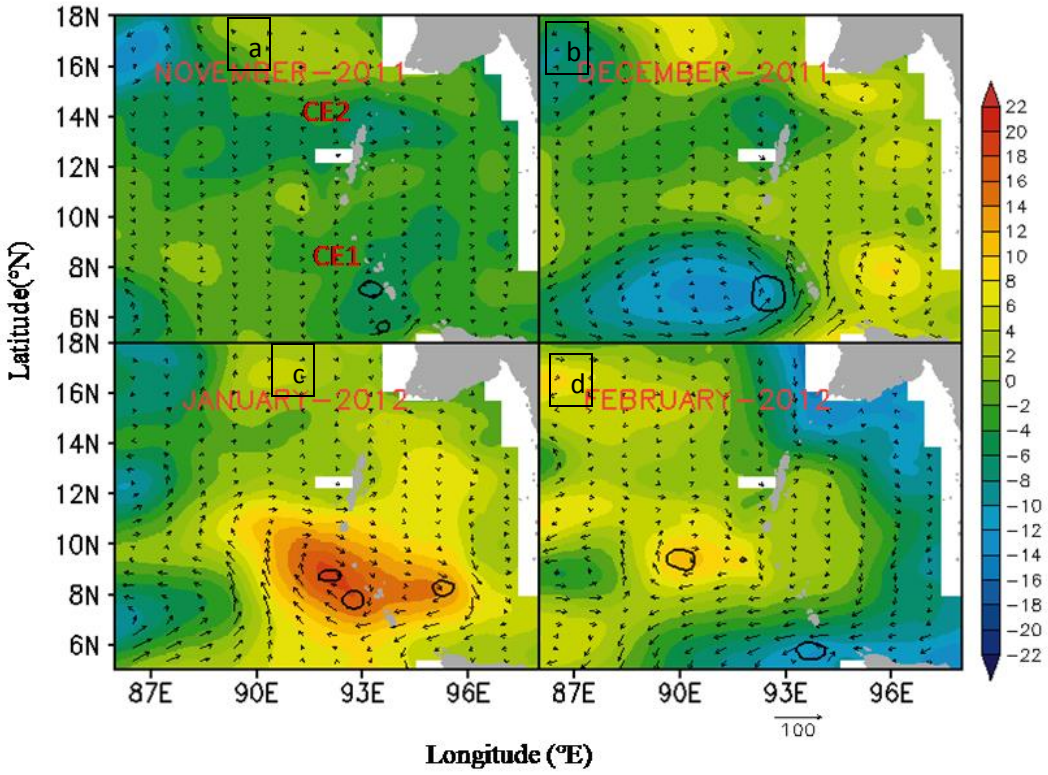

Fig. 7 Merged map of SSHA (m), Geostrophic current (cm/s) and Okubo-Weiss paremeter (Black contour of -2x10-11/s2) from Aviso during a) November b) December c) January d) February

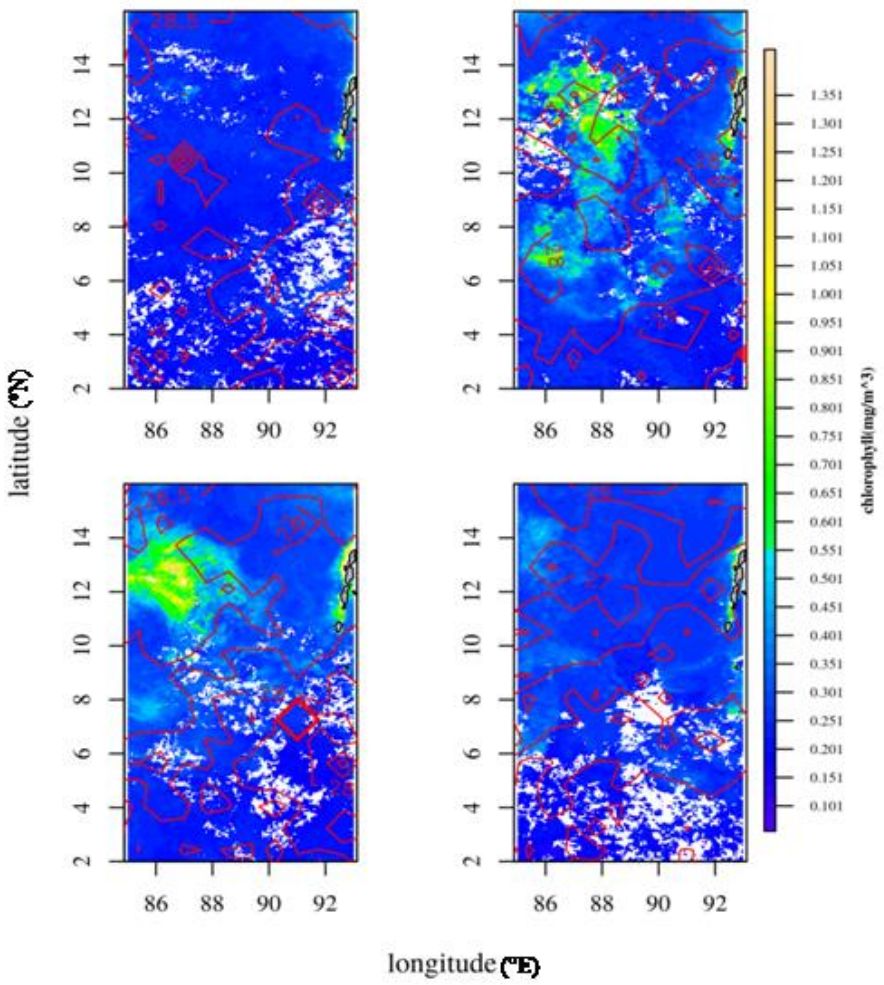

Fig.8 Overlap map of SST (°C-monthly MODIS Aqua) and Chl a (mg/m^3-monthly MODIS Aqua) during a) November, b) December, c) January, d) February